Journal of Institute of Science and Technology, 31(1), 93-106 (2026)
ISSN: 2467-9062 (print), e-ISSN: 2467-9240
https://doi.org/10.3126/jist.v31i1.85935

Research Article

DESIGN, SYNTHESIS, BIOLOGICAL EVALUATION, AND COMPUTATIONAL INSIGHTS OF 1,2,4-TRIAZOLE-BASED SCHIFF AND MANNICH BASE DERIVATIVES INCORPORATING 3,4,5-TRIHYDROXYBENZOIC ACID

Kishor Bhandari[1], Bhushan Shakya[1]*

[1]*Department of Chemistry, Amrit Campus, Tribhuvan University, Nepal*
**Correspondence: bhusansakya@gmail.com*

***(Received**: November 2, 2025; **Revised**: April 19, 2026; **Accepted**: May 25, 2026)*

ABSTRACT

1,2,4-Triazole is a privileged heterocyclic scaffold with various biological activities and extensive pharmaceutical applications. In this work, a series of new Schiff base (5a and 5b) and Mannich base (6a and 6b) derivatives of 1,2,4-triazole incorporating 3,4,5-trihydroxybenzoic acid were synthesized *via* a multi-step synthetic route. Thin Layer Chromatography (TLC), melting point analysis, UV-Vis, FT-IR, ^{1}H-NMR, and ^{13}C-NMR spectroscopy were utilized to verify their molecular framework. The existence of mixture of *E* and *Z* geometric isomers determined by NMR spectral analysis indicated the presence of stereoisomeric diversity in the target compounds. These newly produced compounds were tested concerning their *in vitro* antimicrobial, antioxidant and cytotoxic properties. The Mannich base derivatives (6a and 6b) demonstrated enhanced antimicrobial activity, exhibiting inhibition zones of up to 31 mm against *Bacillus subtilis* and 33 mm against *Saccharomyces cerevisiae*, surpassing the corresponding Schiff bases and showing responses comparable to ciprofloxacin and itraconazole under the tested conditions. In the DPPH assay, compounds 6a and 5a displayed notable radical scavenging activity (IC_{50} = 2.350 and 2.962 mg/mL, respectively), although lower than standard ascorbic acid. Brine shrimp lethality assay indicated concentration-dependent cytotoxicity, with LC_{50} values ranging from 48.39 to 157.90 µg/mL. Quantum chemical calculations (DFT-based geometry optimization, HOMO-LUMO analysis, and molecular electrostatic potential mapping) provided insights into electronic properties and reactive sites. Moreover, ADMET predictions suggested favorable pharmacokinetic profiles and low toxicity risks for most of these synthesized compounds. The present study highlights these triazole-based derivatives as promising candidates for further development in the field of medicinal chemistry.

Keywords*:* 1,2,4-Triazole, Antimicrobial activity, Computational studies, Mannich base, Schiff base

INTRODUCTION

Infections by bacteria and fungi, disorders related to oxidative stress, and abnormal cell growth caused by toxic substances remain serious global health problems. They contribute significantly to morbidity, mortality, and economic burden around the world (Frieri et al., 2017; WHO Bacterial Priority Pathogens List, 2024; Pooja et al., 2025). The rapid development of multidrug-resistant microbial strains has lowered the effectiveness of current antibiotics and antifungal agents (Rouzi et al., 2025). Oxidative stress has also been linked to many chronic conditions, including cardiovascular diseases, neurodegenerative disorders, and diabetes (Nediani et al., 2024). In the early stages of drug discovery, cytotoxicity screening play an essential role to provide insights into the potential therapeutic relevance of compounds, especially in identifying candidates with antiproliferative or anticancer potential (Niksic et al., 2021). These smoldering issues have driven the pursuit of novel, multifunctional bioactive compounds that can simultaneously achieve multiple therapeutic targets.

In order to solve these ongoing biomedical problems, chemists have turned their attention to heterocyclic motifs. Among these, 1,2,4-triazole is notable for its diverse pharmacological activities, such as antibacterial (Yang et al., 2021), antifungal (Sadeghian et al., 2023; Zhu et al., 2023), antioxidant (Peng et al., 2021; Aryal & Shakya, 2023), anticancer (Osmaniye et al., 2021), anti-inflammatory (Azim et al., 2021), and so on. 1,2,4-triazole nucleus plays a key role as a pharmacophore because of its high metabolic stability and features to act as both a hydrogen bond donor and acceptor at receptor active sites. Its polar nature further enhances the solubility of ligand and leads to favorable pharmacokinetic and pharmacodynamic profiles (Kaur et al., 2016). There are numerous clinically used agents based on 1,2,4-triazole scaffold, including fluconazole, itraconazole, posaconazole, voriconazole, ravuconazole,

anastrozole, ribavirin, and estazolam (Aggarwal & Sumran, 2020). Because of its structural adaptability, it can be strategically functionalized to enhance potency, selectivity, and overall therapeutic efficacy by modifying physicochemical and biological properties. It possesses reactive nucleophilic centers, due to why it becomes an excellent starting point for creating various interesting N and S-bridged heterocycles (Wu et al., 2019). The addition of Schiff base or Mannich base functionalities to the triazole framework can further improve lipophilicity, electronic distribution, and binding affinity toward biological targets, as per the principle of active superposition.

Despite the extensive literature on triazole derivatives, the continued rise in drug-resistant pathogens, the burden of oxidative stress–related diseases, and the need for novel cytotoxic agents underscore the demand for new, multifunctional analogues. In this context, the present study was designed to synthesize and characterize the new Schiff base (5a and 5b) and Mannich base (6a and 6b) derivatives of 1,2,4-triazole (Fig. 1), evaluate their *in vitro* antimicrobial, antioxidant, and cytotoxic activities, and complement experimental results with computational analyses, including Density Functional Theory (DFT), and ADMET prediction, to provide deeper insight into their structure-activity relationships and therapeutic potential.

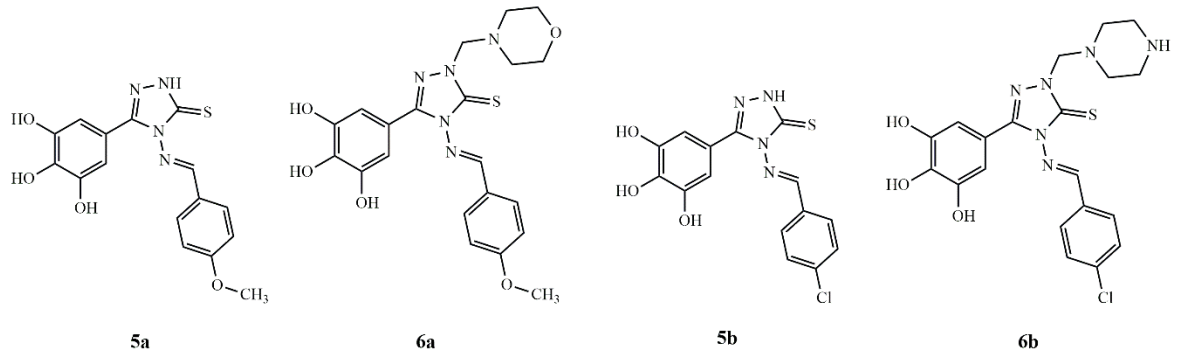

Figure 1. Structure of synthesized title compounds

MATERIALS AND METHODS

Materials

Reagents, starting materials, and solvents were obtained from standard commercial sources, and all chemicals used were of analytical grade. TLC was conducted on silica gel 60 F_{254} plates using *n*-hexane/ethyl acetate, and spots were visualized with iodine vapors. Melting point was measured on an Optics Technology apparatus and reported uncorrected. UV-Vis (200-600 nm) and FT-IR (4000–500 cm^{-1}) spectrum were recorded using Labtronics LT-2802 and Perkin-Elmer Spectrum Two (version 10.6.2) instruments, respectively, at the Department of Chemistry, Amrit Campus, Tribhuvan University, Nepal. NMR spectra were obtained using a Bruker Ascend 400 MHz spectrometer in DMSO-d_6, with chemical shifts in ppm relative to tetramethylsilane (TMS) at Nepal Academy of Science and Technology (NAST), Kathmandu, Nepal. All biological assays were performed at the Himalayan Research Institute of Biotechnology Pvt. Ltd., Kathmandu, Nepal.

Synthesis of target compounds

The synthetic route is illustrated in supplementary information Figure S1. At first, 4-amino-3-(3,4,5-trihydroxyphenyl)-1,2,4-triazole-5-thione (04T) was prepared from gallic acid by esterification followed by treatment with hydrazine monohydrate and carbon disulfide in subsequent steps. The Schiff bases (5a and 5b) were prepared by the condensation reaction between 04T with *p*-anisaldehyde and *p*-chlorobenzaldehyde, respectively. Mannich reaction of the Schiff bases using desired amine produced the Mannich bases (6a and 6b). Structures of all synthesized compounds were established using UV-visible, FTIR, and NMR spectroscopic data. The detailed procedure, % yield, physical properties and spectral data are presented in supplementary information (S1–S7).

Biological evaluation

Antimicrobial activity

The synthesized compounds (5a, 6a, 5b, and 6b) were evaluated for their antimicrobial properties against different bacterial strains, including *Escherichia coli*

(ATCC8739), *Klebsiella pneumonia* (ATCC 700603), *Bacillus subtilis* (ATCC 6051), *Staphylococcus aureus* (ATCC6538P), as well as fungal strains such as *Candida albicans* (ATCC2091), and *Saccharomyces cerevisiae* (ATCC18824) using the agar well diffusion method. Mueller-Hinton agar (MHA) was used for bacterial strains and *C. albicans*, while Sabouraud dextrose agar (SDA) was used for *S. cerevisiae*. Test solutions (100 mg/mL for bacteria and *C. albicans*, 50 mg/mL for *S. cerevisiae*) were prepared in dimethylsulphoxide (DMSO). Ciprofloxacin (1 mg/mL, 10 µL) and itraconazole (20 mg/mL for *C. albicans*, 15 mg/mL for *S. cerevisiae*; 10 µL) served as positive controls, with DMSO as the negative control. Wells (9 mm diameter, 3 mm depth) were loaded with 100 µL of the respective solutions, and plates were incubated at 37 °C for 24 h (*bacteria*, *C. albicans*) or 48 h (*S. cerevisiae*). Antimicrobial activity was assessed by measuring the diameter of inhibition zones (mm).

Antioxidant activity

The DPPH radical scavenging activity (RSA) of compounds 5a, 5b, 6a, and 6b was determined following a reported method with slight modification mentioned in literature (Brand-Williams et al., 1995). A 0.2 mM DPPH solution was prepared by dissolving 7.8 mg DPPH in 100 mL absolute ethanol and stored at 4 °C. Sample solutions (10–2 mg/mL in ethanol) were prepared, and 1 mL of each was mixed with 3 mL of DPPH solution, shaken, and incubated at 30 °C in the dark for 30 min. Ascorbic acid (2–0.0625 mg/mL) served as the reference standard. Absorbance was measured at 517 nm against ethanol as blank, and % RSA was calculated using:

$$\% \text{ radical scavenging activity (RSA)} = \frac{A_{\text{control}} - A_{\text{sample}}}{A_{\text{control}}} \times 100 \quad \ldots (1)$$

Where, A_{control} and A_{sample} are absorbance of DPPH without sample and absorbance of DPPH incubated with sample concentration, respectively. All assays were performed in triplicate.

Cytotoxicity assay

The brine shrimp lethality assay was performed following standard methodology with minor modifications reported in literature (Apu et al., 2010). Artificial seawater (30 g/L) was prepared, and 100 mg brine shrimp eggs were incubated at 22–29 °C with continuous aeration. After 48 h, hatched nauplii were collected and transferred (20 nauplii/well) into 96-well plates. Test compounds were dissolved in DMSO and diluted with distilled water to prepare a 1000 µg/mL stock, followed by serial dilutions (10–800 µg/mL). Twenty nauplii in seawater were transferred to each well, followed by the addition of 0.4 mL of the respective diluted sample. Plates were incubated for 24 h, with close monitoring during the first 8 h. All tests were performed in triplicate. Mortality was recorded, and percentage lethality was calculated as:

$$\% \text{ Mortality} = \frac{\text{Number of dead nauplii}}{\text{Total number of nauplli}} \times 100 \quad \ldots (2)$$

Computational studies

Density Functional Theory (DFT) calculation

To rationalize the experimental findings, complement computational studies were conducted on the *E*-isomer of the newly synthesized compound. All molecular structures were initially drawn in ChemDraw, and their corresponding SMILES notations were generated and transferred to Avogadro software to construct the initial three-dimensional geometries. The generated structures were then subjected to preliminary geometry optimization using the UFF force field. Energy minimization was carried out using conjugate gradient algorithms until convergence was achieved under default settings. This pre-optimization step ensured that the structures were free from unfavorable steric interactions and provided reasonable starting geometries for subsequent DFT calculations. Geometry optimizations and frequency analyses were performed using Density Functional Theory (DFT) at the B3LYP/6-31G + (d,p) level in the gas phase, as implemented in Gaussian 09 software package, with no symmetry constraints. The selected hybrid functional (B3LYP) and basis set (6-31G + (d,p)) provides a good balance between computational cost and accuracy, and has been widely used for geometry optimization and electronic property calculations of organic molecules. It is particularly suitable for systems containing C, H, N, and O atoms, and has been reported to yield reliable results for molecular structure and reactivity descriptors (Tyagi et al., 2017). To validate the reliability of the employed computational protocol, the selected level of theory (B3LYP/6-31G+(d,p)) was chosen based on its extensive prior use in the study of heterocyclic and triazole-based systems, where it has demonstrated a good balance between computational efficiency and accuracy in predicting molecular geometries and electronic properties. Frequency calculations were performed for all optimized structures, and the absence of imaginary frequencies confirmed that the obtained geometries correspond to true minima on the potential energy surface. This validation ensures that the computed structural and electronic parameters are reliable for further interpretation (Tyagi et al., 2017;

Wu et al., 2019; Qi et al., 2020). Frontier molecular orbitals (HOMO and LUMO) and the corresponding energy gaps ($\Delta E = E_{LUMO} - E_{HOMO}$) were evaluated to assess electronic properties and chemical reactivity. Molecular electrostatic potential (MEP) maps were generated from the optimized geometries to visualize charge distribution and identify potential reactive sites, with surfaces rendered in GaussView 6.0 visualization tool.

In silico pharmacokinetic ADME and toxicity studies

SwissADME and pkCSM online web servers were employed to predict the ADME (Absorption, Distribution, Metabolism, and Excretion) parameters, toxicity profiles, and drug-likeness criteria of the newly designed compounds. These *in silico* predictions provided crucial insights into their pharmacological behavior and synthetic feasibility, supporting their candidacy for further development in drug discovery.

RESULTS AND DISCUSSION

Synthesis

A series of Schiff and Mannich base derivatives of 1,2,4-triazole were synthesized *via* a multi-step synthetic route (Fig. S1), and their structures were confirmed by spectroscopic analyses. The UV-Vis spectra of all compounds displayed absorption bands at λ_{max} 326–344 nm, attributable to $\pi \rightarrow \pi^*$ and $n \rightarrow \pi^*$ transitions of the conjugated triazole-thione system, with 6b showing only an $n \rightarrow \pi^*$ band at 342 nm. FT-IR spectra showed broad O–H stretches (3493-3200 cm^{-1}), characteristic HC=N (azomethine) bands at 1706-1608 cm^{-1}, aromatic C=C (1613–1452 cm^{-1}), C–N (1373–1294 cm^{-1}), phenolic C–O (1289–1202 cm^{-1}), N–C=S (1187–1054 cm^{-1}), and C–Cl (791–720 cm^{-1}) in halogenated derivatives, confirming the presence of hydroxyl, aromatic, azomethine, and thione functionalities. In the ^1H NMR spectra, singlets at δ 10.00–8.55 ppm correspond to the azomethine proton (HC=N), while aromatic protons appeared at δ 7.94–6.38 ppm, and the phenolic OH resonated at δ 5.75–4.36 ppm. The ^{13}C NMR spectra displayed signals at δ 167.49–145.36 ppm for imine carbons (C=N), δ 145.62–101.34 ppm for aromatic carbons, δ 192.15–186.72 ppm for thiocabonyl group (C=S), δ 170.37–147.72 for azomethine carbons (HC=N), and δ 66.01–42.89 ppm for methylene (CH_2) in Mannich base derivatives. Duplication of selected ^1H and ^{13}C signals confirmed the coexistence of *E*/*Z* isomers, consistent with the proposed molecular frameworks.

Biological evaluation

Antibacterial activity

The results of the antibacterial tests (Fig. 2a) showed a clear trend: the Mannich base derivatives 6a and 6b were more active than their corresponding Schiff bases, 5a and 5b, across all examined bacterial strains. Among the compounds, 6a showed the highest inhibitory effect in term of zone diameter. It generated a 31 mm inhibition zone against *B. subtilis*, exceeding the response of the standard drug ciprofloxacin, and produced a 24 mm zone of inhibition against *K. pneumoniae*. The enhanced performance of 6a may arise from the morpholine group, whose basic and hydrophilic nature can promote better solubility, facilitate penetration through bacterial membranes, and support stronger interactions with intracellular targets. Compound 6b also displayed notable activity, particularly toward *K. pneumoniae* (25 mm) and *B. subtilis* (27 mm), which is consistent with the hydrogen-bonding capacity and electrostatic characteristics associated with its piperazine moiety. In contrast, Schiff bases 5a and 5b exhibited only modest effects, with 5b being the least active. Its weaker response is likely linked to the electron-withdrawing chlorine substituent and its comparatively poor solubility. Taken together, these findings highlight the advantage of incorporating nitrogen-rich, polar heterocycles to improve aqueous solubility, cellular uptake, and interactions with bacterial targets, ultimately leading to stronger antibacterial action.

Antifungal activity

The antifungal evaluation against *Candida albicans* and *Saccharomyces cerevisiae* (Fig. 2b) showed a clear structure-activity relationship. The Mannich bases 6a and 6b produces larger zones of inhibition than the standard drug itraconazole under the tested conditions. Compound 6a exhibited inhibition zones of 30 mm for *C. albicans* and 29 mm for *S. cerevisiae*, both higher than the control (21 mm and 25 mm). This strong effect may be due to the morpholine ring, which is basic and hydrophilic. These features can help the compound pass through the fungal cell wall and interact with important enzymes, possibly affecting ergosterol formation or damaging the membrane. Compound 6b was the most active among the synthesized derivatives. It produced a 33 mm zone against *S. cerevisiae* and 26 mm against *C. albicans*. Its piperazine ring has two nitrogen atoms, giving it both flexibility and better interaction with enzymes and cell membranes. In contrast, compound 5a, which contains a methoxy group, showed only moderate activity (20 mm and 18 mm). This may be due to its

lower polarity and poor solubility, which limit its interaction with fungal targets. Compound 5b, with a chlorine group, had the weakest activity (19 mm and 17 mm). The chlorine atom makes the compound more hydrophobic and reduces its ability to form useful interactions. Overall, the results show that polar, nitrogen-containing rings greatly improve antifungal activity in these triazole derivatives.

Antioxidant activity

The antioxidant potential of the synthesized compounds was evaluated using the DPPH free radical scavenging assay, and the results are presented in terms of IC_{50} values calculated using nonlinear regression analysis employing a four-parameter logistic (4PL) model implemented in GraphPad Prism 10.4.2, as illustrated in Figure 2c. Among the synthesized derivatives, 6a exhibited the highest antioxidant activity within the series, as indicated by its comparatively lower IC_{50} value (IC_{50} = 2.350 mg/mL, R^2 = 0.9928), followed by 5a (IC_{50} = 2.962 mg/mL, R^2 = 0.9972). However, under the experimental condition, the overall activity remains in the weak range, based on standard IC_{50} criteria. The strong activity of compound 6a among the studied compounds may be due to the combined effect of its methoxy group and the polar morpholine ring, which help it dissolve better and react more easily with free radicals. In contrast, 6b (IC_{50} = 4.249 mg/mL, R^2 = 0.9951) and 5b (IC_{50} = 6.056 mg/mL, R^2 = 0.9967) showed reduced activity, consistent with the electron-withdrawing effect of chlorine, which diminishes electron/hydrogen donation capacity despite the presence of solubilizing nitrogenous side chains. The reference ascorbic acid displayed the expected highest activity (IC_{50} = 0.054 mg/mL, R^2 = 0.9961). All these outcomes confirmed that compounds with electron-donating groups like $–OCH_3$ and polar rings have comparatively higher antioxidant activity within the series, while electron-withdrawing groups like –Cl reduces it.

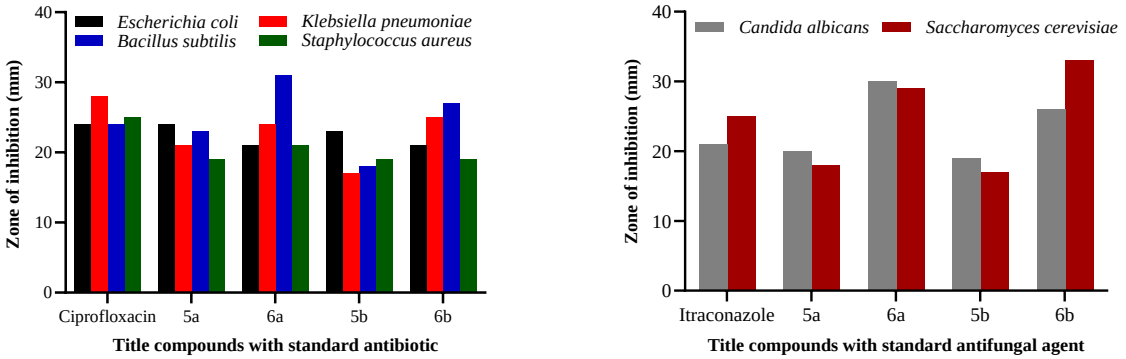

(a)

(b)

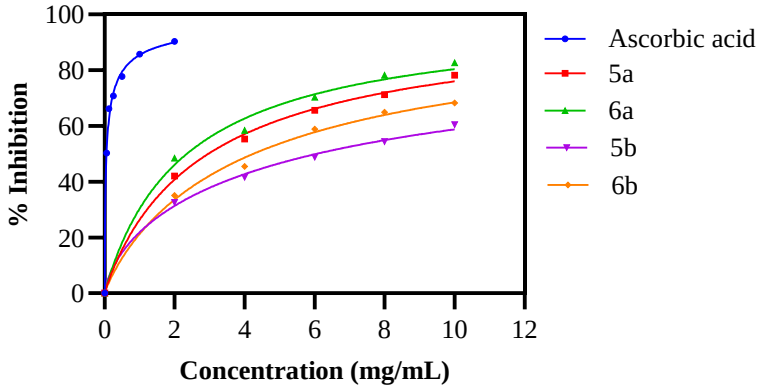

(c)

Figure 2. Biological activities of synthesized compounds (a) Antibacterial activities (b) Antifungal activities (c) Antioxidant activities

Cytotoxicity assay

The dose-response of all compounds against *Artemia salina* nauplii, along with the LC_{50} values calculated using nonlinear regression (4PL model, GraphPad Prism 10.4.2), and expressed with their corresponding 95% confidence intervals (CI), is shown in Figure 3. All compounds caused mortality in a concentration-dependent manner. Compound 5a, which has a *p*-methoxyphenyl group, showed the weakest cytotoxicity (LC_{50} = 157.90 µg/mL), likely due to poor membrane permeability and limited interaction with targets. The addition of a morpholine ring in 6a increased activity (LC_{50} = 87.82 µg/mL), suggesting that greater polarity and hydrogen-bonding ability improve bioavailability. The *p*-chlorophenyl compound 5b slightly showed enhanced activity (LC_{50} = 87.53 µg/mL), probably because the halogen increases lipophilicity and hydrophobic binding. The most active compound, 6b, has both a *p*-chlorophenyl group and a piperazine ring, showing an LC_{50} of 48.39 µg/mL. This higher activity may result from the combined effects of lipophilicity, basicity, and hydrogen-bonding, which enhances uptake and intracellular binding. Notably, LC_{50} reflects the full dose-response curve, not just a single concentration, highlighting the significance of the curve in measuring potency. Overall, the cytotoxicity followed the order: 6b > 5b > 6a > 5a, showing that halogen substitution and heterocyclic modifications improve activity.

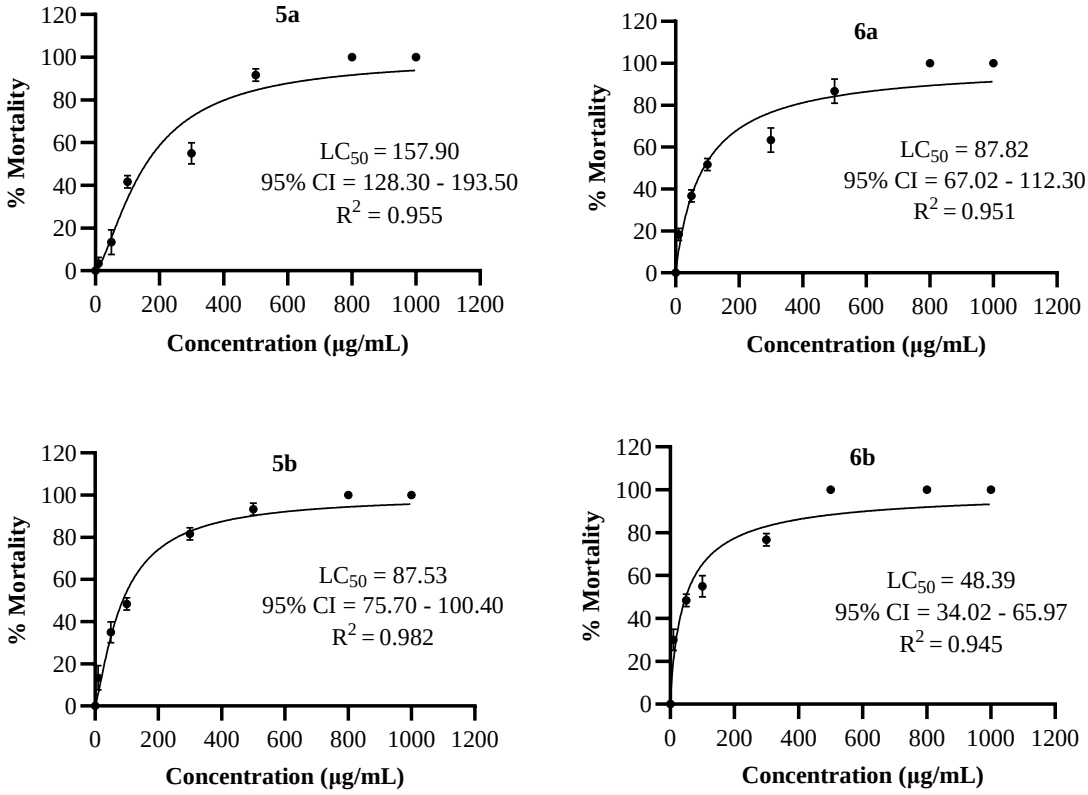

Figure 3. Dose-response curves representing cytotoxicity of title compounds

Computational studies

Density Functional Theory (DFT) calculation

Density functional theory (DFT) calculations were performed at 0 K, which corresponds to the electronic ground-state energy at the optimized geometry without explicit thermal contributions. However, the computed electronic properties, such as HOMO–LUMO energy gaps, charge distribution, and molecular electrostatic potential, are primarily governed by the electronic structure and are only weakly dependent on temperature. At room temperature (298 K), the thermal energy ($kBT \approx 0.026$ eV) is relatively small compared to the energy differences between molecular orbitals, indicating that the qualitative trends in reactivity and electronic behavior remain largely unaffected. Therefore, the 0 K DFT results are considered representative for interpreting molecular properties under ambient conditions (Wang et al., 2021).

Furthermore, although temperature-dependent corrections (e.g., vibrational and entropic contributions from frequency calculations) can refine absolute thermodynamic quantities, such effects are generally small and tend to cancel out when comparing structurally similar compounds. In the present study, the conclusions are based on relative electronic descriptors and trends, which are expected to remain valid across the 0–298 K range (Liu et al., 2024).

Geometry optimization

The vibrational frequency analysis showed no imaginary frequencies, confirming that all optimized geometries are true minima on the potential energy surface. The optimized structures are shown in Figure 4.

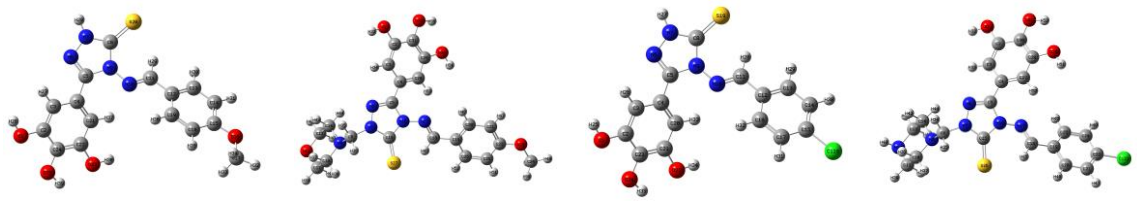

(5a) **(6a)** **(5b)** **(6b)**

Figure 4. Optimized geometric configuration of title compounds

Table 1. Optimized geometric parameters of title compounds

Compounds	Parameters	Bond length (Å)	Compounds	Parameters	Bond Angle (°)
5a	C(5)=N(6)	1.3112	**5a**	C(22)=C(24)-C(2)	118.6094
	N(6)-N(7)	1.3634		C(5)=N(6)-N(7)	104.5845
	N(7)-C(8)	1.3570		N(7)-C(8)=S(20)	126.7141
	C(8)=S(20)	1.6749		C(8)-N(9)-N(10)	128.6208
	N(9)-N(10)	1.3847		N(9)-N(10)=C(11)	117.3156
	N(10)=C(11)	1.2917			
6a	C(5)=N(6)	1.3107	**6a**	C(2)-C(31)=C(29)	118.5749
	N(6)-N(7)	1.3690		C(5)=N(6)-N(7)	105.5354
	N(7)-C(15)	1.3636		N(7)-C(15)=S(27)	127.5419
	C(15)=S(27)	1.6773		C(15)-N(16)-N(17)	128.5300
	N(16)-N(17)	1.3857		N(16)-N(17)=C(18)	117.1997
	N(17)=C(18)	1.2915		N(7)-C(8)-N(9)	112.4948
	N(7)-C(8)	1.4579			
	C(8)-N(9)	1.4489			
5b	C(5)=N(6)	1.3094	**5b**	C(21)=C(23)-C(2)	118.6637
	N(6)-N(7)	1.3640		C(5)=N(6)-N(7)	104.7003
	N(7)-C(8)	1.3565		N(7)-C(8)=S(19)	126.2343
	C(8)=S(19)	1.6748		C(8)-N(9)-N(10)	130.3225
	N(9)-N(10)	1.3770		N(9)-N(10)=C(11)	119.3434
	N(10)=C(11)	1.2897			
6b	C(5)=N(6)	1.3084	**6b**	C(28)=C(30)-C(2)	118.6277
	N(6)-N(7)	1.3691		C(5)=N(6)-N(7)	105.6310
	N(7)-C(15)	1.3630		N(7)-C(15)=S(26)	126.9845
	C(15)=S(26)	1.6772		C(15)-N(16)-N(17)	130.7651
	N(16)-N(17)	1.3765		N(16)-N(17)=C(18)	119.8930
	N(17)=C(18)	1.2895		N(7)-C(8)-N(9)	112.5298
	N(7)-C(8)	1.4607			
	C(8)-N(9)	1.4468			

Overall, the compounds had similar bond lengths and angles, reflecting a conserved central heterocyclic core, with slight differences depending on the substituents. The imine (C=N) bonds averaged about 1.31 Å, while the N–N bonds were slightly longer (1.36–1.38 Å), consistent with their electronic environments. The thioamide (C=S) bonds were around 1.67 Å in all derivatives, suggesting stable conjugation with neighboring atoms. In 6a and 6b, some N–C bonds in the triazole ring were slightly longer, likely due to steric and electronic effects from the phenyl substituents. Key bond angles, such as C=N–N and N–C=S, ranged from approximately 104° to 130° (Table 1), showing slightly distorted but conjugated rings. These structural features indicate planarity and rigidity, which are often important for effective target binding and biological activity.

The optimized bond lengths and bond angles obtained in this study are in good agreement with previously reported DFT studies on structurally related 1,2,4-triazole derivatives (Tyagi et al., 2017; Wu et al., 2019; Qi et al., 2020), further supporting the validity and robustness of the applied computational methodology.

Frontier molecular orbital analysis

Frontier Molecular Orbital (FMO) theory reveals that the highest occupied molecular orbital (HOMO) and the lowest unoccupied molecular orbital (LUMO) are important to determine the compound's biological activity. The HOMO donates electrons, while the LUMO accepts them (Qi et al., 2020; Wu et al., 2020). To understand how the compounds might act, the energies of these orbitals were calculated (Fig. 5). The energy difference between LUMO and HOMO (ΔE) reflects the molecule's chemical hardness or softness. A smaller ΔE usually means the molecule is more reactive, less stable, and more likely to interact with biological targets because electron transfer is easier (Parr & Yang, 2020). The green and red regions in the molecular orbital plots represent opposite phases of the orbital wavefunction. These phases indicate the sign of the wavefunction and are used to describe constructive or destructive overlap, rather than representing positive or negative charge.

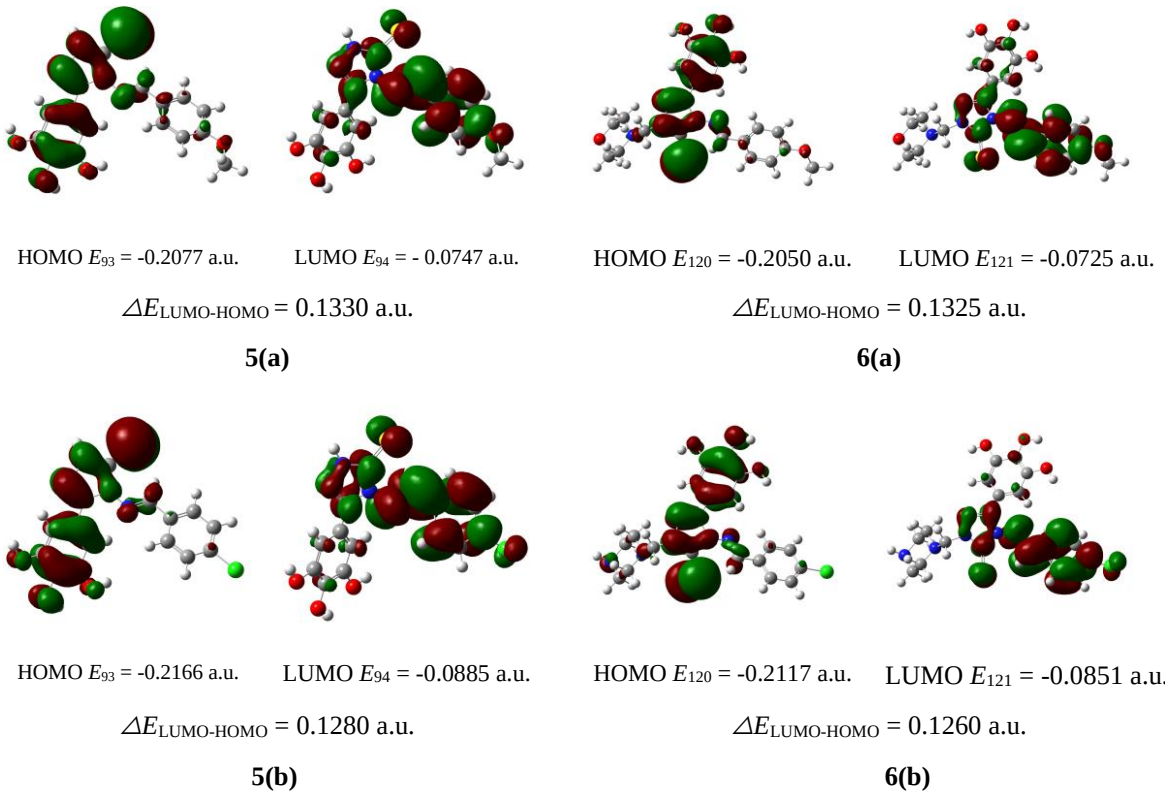

Figure 5. LUMO and HOMO maps of title compounds from B3LYP/6-31G + (d,p). Green: positive molecular orbitals; Red: negative molecular orbitals

In all four compounds, the HOMO is predominantly localized over the electron-rich 3,4,5-trihydroxyphenyl ring and the triazole linkage (–C=N–NH–C=S), indicating contributions from phenolic hydroxyl groups and lone pairs on nitrogen and sulfur atoms. In 5a**,** the HOMO is concentrated on the phenolic ring and triazole nucleus, while the LUMO extends over the triazole and para-methoxyphenyl ring, suggesting π–π* conjugation and intramolecular charge transfer (ICT). In 6a, incorporation of a morpholine-based Mannich moiety increases electron delocalization *via* nitrogen and oxygen lone pairs, resulting in an extended HOMO–LUMO delocalization pathway and a slightly reduced *ΔE*, indicative of enhanced reactivity. In 5b, substitution with a *p*-chlorophenyl group maintains a HOMO distribution similar to 5a, but the LUMO is localized on the electron-deficient chlorophenyl ring. The inductive electron-withdrawing effect of chlorine lowers *ΔE* and increases electrophilic reactivity. In 6b, the Mannich derivative of 5b with a piperazine group, the electrons are delocalized across the piperazine, triazole, and chlorophenyl parts. The HOMO is mainly over the nitrogen-rich regions, while the LUMO is focused on the triazole and chlorophenyl rings. This compound has the smallest *ΔE* (0.1260 a.u.) among all the derivatives, showing the highest chemical reactivity and electron transfer potential. Overall, the FMO analysis shows that the Mannich bases 6a and 6b have better orbital delocalization and higher reactivity than their parent Schiff bases, which may explain their stronger biological activity or better binding.

Molecular electrostatic potential (MEP) analysis

Molecular electrostatic potential (MEP) indicates which parts of a molecule are likely to act as electron-rich (nucleophilic) or electron-poor (electrophilic) regions. In general, positive areas on a molecule tend to interact with negative areas on other molecules, and the larger the charge difference, the stronger the interaction (Wu et al., 2019). MEP maps are also useful for understanding how molecules can interact with proteins or participate in other intermolecular forces (Wu et al., 2020). Figure 6 shows the MEP maps of the compounds studied.

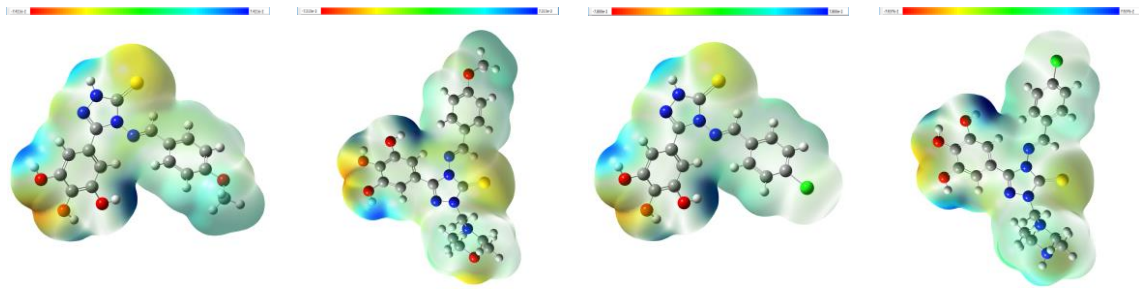

(5a) **(6a)** **(5b)** **(6b)**

Figure 6. MEP maps of title compounds. Red color indicates electron-rich (nucleophilic) regions, blue indicates electron-deficient (electrophilic) regions, and green/yellow represents areas of moderate potential

MEP maps of all four compounds showed relatively negative potential (orange to light red regions) around phenolic –OH groups. This indicates a strong nucleophilic character and potential to act as hydrogen-bond donors. In addition, high electron density was observed on the triazole thione sulfur and hydrazone nitrogen, which further supports their role as reactive sites. A comparative analysis of the MEP maps reveals clear differences in charge distribution among the synthesized compounds. In compounds 5a and 5b (Schiff bases), the negative electrostatic potential is mainly localized around the phenolic –OH groups and the thione (C=S) moiety, while the rest of the molecular surface remains relatively neutral, indicating limited charge separation. In 5a, electron density is primarily concentrated on the 3,4,5-trihydroxyphenyl ring, whereas in 5b, the presence of the electron-withdrawing chloro substituent slightly enhances charge localization without significantly increasing overall polarity. In contrast, the Mannich base derivatives 6a and 6b exhibit a more extensive distribution of both negative and positive regions across the molecular surface. In 6a, the morpholine ring introduces additional electron-rich (due to heteroatoms) and electron-deficient regions, increasing overall polarity and enabling more

potential interaction sites. Similarly, in 6b, the piperazine moiety contributes multiple nitrogen centers, leading to a broader distribution of electrostatic potential and enhanced charge separation. These results suggest that the Mannich bases 6a and 6b have higher surface polarity, more nucleophilic and electrophilic centers, and greater charge separation than the parent Schiff bases (5a and 5b) which may contribute to their improved interaction with biological targets and enhanced biological activity.

A comparison between the MEP and HOMO distributions of compound 5a reveals that these descriptors provide complementary information. The oxygen-containing region exhibits a relatively negative electrostatic potential (red/orange in the MEP surface) due to the high electronegativity of oxygen atoms; however, the HOMO density in this region is comparatively small. This suggests that, although electron-rich, these sites are not the primary contributors to the highest occupied molecular orbital, likely due to electron-withdrawing effects or resonance stabilization. In contrast, the sulfur atom displays a larger HOMO lobe, indicating a significant contribution to the frontier orbital and a greater tendency to donate electrons, even though its MEP is less negative. This difference highlights that MEP reflects electrostatic charge distribution, whereas HOMO describes orbital participation, and the two are not necessarily directly correlated.

In silico pharmacokinetic ADME and toxicity analysis

Drug-like properties

Assessing the pharmacokinetic characteristics of a compound is a crucial step in evaluating its potential as a therapeutic agent. To estimate the oral bioavailability of the proposed inhibitors, their drug-likeness was analyzed using Lipinski's Rule of Five. In addition to Lipinski's criteria, other descriptors based on Veber's rule, such as topological polar surface area (TPSA) and the number of rotatable bonds, were also evaluated to provide a more comprehensive assessment of pharmacokinetic properties. Compounds with favorable bioavailability typically possess a molecular weight under 500 Da, a logP value ≤5, fewer than 5 hydrogen bond donors, fewer than 10 hydrogen bond acceptors, no more than 10 rotatable bonds, and a topological polar surface area below 140 Å^2. A compound is generally considered orally active if it fulfills at least three of these five criteria (Bouamrane et al., 2024; Kurmi & Karati, 2025). As summarized in Table 2, the evaluated molecules complied with Lipinski's parameters, although they had one violation in terms of TPSA, suggesting that the newly developed compounds exhibit promising oral bioavailability.

Table 2. The Lipinski properties of target compounds

Compounds	Properties					
	LogP	**HBD**	**HBA**	**TPSA (Å^2)**	**nrotb**	**MW**
5a	2.240	4	6	147.98	4	358.37
6a	1.980	3	8	149.59	6	457.50
5b	2.740	4	5	138.75	3	362.79
6b	2.290	4	7	143.16	5	460.94

LogP: logarithm of partition coefficient of compound between *n*-octanol and water, HBD: number of hydrogen bond donor, HBA: number of hydrogen bond acceptor, TPSA: Topological Polar Surface Area, nrotb: number of rotatable bonds, MW: Molecular Weight

ADME analysis

The ADME profile of newly synthesized compounds was evaluated using in silico predictive models, and the summarized data are shown in Table 3.

Table 3. *In Silico* ADME predictions of synthesized compounds

Models	Compounds			
	5a	**6a**	**5b**	**6b**
Water solubility Numeric (log mol/L)	-2.954	-3.180	-2.962	-3.185

Caco-2 permeability Numeric (log papp in 10^{-6} cm/s)	-0.285	0.222	-0.37	-0.075
Intestinal absorption (human) Numeric (% Absorbed)	64.608	73.779	67.276	67.261
Skin permeability Numeric (log *K*p)	-2.735	-2.739	-2.735	-2.736
p-glycoprotein substrate Categorical (Yes/No)	Yes	Yes	Yes	Yes
p-glycoprotein I/II inhibitor Categorical (Yes/No)	No/No	No/No	No/No	No/Yes
VDss (human) Numeric (log L/kg)	-0.084	1.027	-0.258	1.686
BBB permeability Numeric (log BB)	-1.902	-1.445	-1.874	1.686
CNS permeability Numeric (log PS)	-2.83	-3.469	-2.526	-2.71
CYP2D6 substrate Categorical (Yes/No)	Yes	No	Yes	No
CYP3A4 substrate Categorical (Yes/No)	No	Yes	No	Yes
CYP1A2 inhibitor Categorical (Yes/No)	Yes	No	Yes	No
CYP2C19 inhibitor Categorical (Yes/No)	No	No	Yes	No
CYP2C9 inhibitor Categorical (Yes/No)	No	Yes	Yes	Yes
CYP2D6 inhibitor Categorical (Yes/No)	No	No	No	No
CYP3A4 inhibitor Categorical (Yes/No)	No	Yes	No	No
Total Clearance Numeric (log ml/min/kg)	0.044	0.557	-0.004	0.332

VDss: Steady state volume of distribution, BBB: Blood-brain barrier, CNS: central nervous system, CYP2D6: Cytochrome P450 family 2 subfamily D member 6, CYP3A4: Cytochrome P450 family 3 subfamily A member 4, CYP1A2: Cytochrome P450 family 1 subfamily A member 2, CYP2C19: Cytochrome P450 family 2 subfamily C member 19, CYP2C9: Cytochrome P450 family 2 subfamily C member 9, CYP2C19: Cytochrome P450 family 2 subfamily C member 19

To facilitate interpretation of the predicted ADMET parameters, commonly accepted reference ranges were considered. Compounds with water solubility values (log mol/L) between -2 and -4 are generally regarded as moderately soluble and suitable for oral drugs. In this study, all compounds (-2.954 to -3.185) fall within this range, indicating acceptable solubility. Caco-2 permeability values greater than 0 are indicative of good intestinal permeability, while values below -0.5 suggest poor permeability. Among the synthesized compounds, **6a** (0.222) exhibits good permeability, whereas the remaining compounds show moderate to low permeability. Human intestinal absorption above 60% is typically considered favorable for oral bioavailability; all compounds (64.608–73.779%) satisfy this criterion. Skin permeability (log Kp) values around -2.5 indicate low transdermal penetration, and all compounds (-2.735 to -2.739) fall within this range, suggesting minimal dermal absorption (Neupane et al., 2025; Pires et al., 2015). All analogs were predicted to be p-glycoprotein (P-gp) substrates, although none inhibited P-gp I; only 6b showed potential inhibition of P-gp II, which may influence multidrug resistance. The values of steady-state volume of distribution (VDss = 1.686 log L/kg) and positive BBB permeability (log BB = 1.686) of 6b indicated possible CNS penetration, and other compounds were negatively predicted to penetrate the brain. CNS permeability (log PS) of 6a (-3.469) and 5b (-2.526) were the lowest and highest, respectively. Cytochrome P450 (CYP) enzymes play a crucial role in drug metabolism and detoxification, primarily through oxidative phase I biotransformation. Compounds acting as CYP substrates are subjected to metabolic processing, which significantly influence their clearance, half-life, and oral bioavailability. In the present study, compounds 5a and 5b were

predicted to be substrates of CYP2D6, whereas 6a and 6b were identified as CYP3A4 substrates, indicating that these molecules are likely to undergo hepatic metabolism *via* major and well-characterized enzymatic pathways. Inhibition of CYP enzymes, particularly CYP3A4, CYP2C9, and CYP1A2, may lead to drug–drug interactions by interfering with the metabolism of co-administered drugs. The studied compounds exhibited selective inhibition profiles, where individual analogues inhibited specific CYP isoforms (e.g., CYP1A2, CYP2C9, or CYP3A4) without demonstrating broad-spectrum inhibition across all major CYP enzymes. Such selectivity suggests a moderate interaction potential rather than severe metabolic liability. Notably, none of the compounds were predicted to inhibit CYP2D6, which is advantageous given its polymorphic nature and clinical relevance in interindividual variability. Overall, the presence of CYP substrate characteristics along with selective enzyme inhibition is commonly observed in drug-like molecules and reflects metabolically competent structures. These findings suggest that the synthesized compounds possess acceptable metabolic behavior for early-stage drug development; however, further *in vitro* and *in vivo* investigations are necessary to comprehensively evaluate their metabolic stability and potential for drug–drug interactions. It was predicted that clearance was the most in 6a (0.557 log mL/min/kg), which would result in faster elimination and 5b exhibited the lowest (-0.004) implying the longest systemic retention.

Toxicity prediction and safety profiling

The predicted toxicity profiles of the synthesized compounds are summarized in Table 4. These data provide a preliminary safety assessment for evaluating the compounds therapeutic potential.

Table 4. *In Silico* toxicity profile of synthesized compounds

Compounds	AMES test	Max. tolerated dose (human)	hERG I/II inhibitor	Oral Rat Acute Toxicity (LD_{50})	Oral Rat Chronic Toxicity (LOAEL)	Skin Sensitization
	Categorical (Yes/No)	Numeric (log mg $kg^{-1}day^{-1}$)	Categorical (Yes/No)	Numeric (mol kg^{-1})	Numeric (log mg $kg^{-1}bw^{-1}day^{-1}$)	Categorical (Yes/No)
5a	No	0.856	No/Yes	2.743	2.604	No
6a	No	0.429	No/Yes	2.624	2.04	No
5b	No	0.841	No/Yes	2.781	2.572	No
6b	No	0.584	No/Yes	2.894	2.433	No

The genotoxic risk was low with all compounds predicted to be non-mutagenic in the AMES test. The maximum tolerated dose (MTD) in humans ranged from 0.429 to 0.856 log mg $kg^{-1}day^{-1}$ with the highest predicted tolerance at 5a and lowest at 6a. None of the analogs were predicted to inhibit hERG I; however, all compounds showed potential inhibition of hERG II, suggesting a possible risk of off-target cardiac side effects. The predicted hERG II liability for all four compounds may be attributed to shared structural features, such as the presence of aromatic moieties and heteroatoms, which are known to interact with the hERG potassium channel. In addition, physicochemical properties, including lipophilicity and electronic distribution, may further contribute to this behavior. Nevertheless, it is important to note that hERG II classification reflects a moderate risk based on computational predictions and does not necessarily indicate actual cardiotoxicity. Therefore, these findings should be interpreted with caution and require further experimental validation. The predicted oral rat acute toxicity (LD_{50}) values were 2.624–2.894 mol kg^{-1} where 6b was the least acutely toxic and 6a the most acutely toxic. Chronic toxicity, assessed *via* LOAEL, was highest for 5a (2.604 log mg $kg^{-1}bw^{-1}day^{-1}$), further supporting its comparatively favorable safety profile. No compound was anticipated to produce any skin sensitization and thus the risk of dermal allergic reactions was minimal.

CONCLUSION

In this exploration, a series of new Schiff bases (5a and 5b) and Mannich bases (6a and 6b) of 1,2,4-triazole were prepared from 3,4,5-trihydroxybenzoic acid through a multi-step reaction. The compounds were obtained in good yields and high purity. Their structures were confirmed using UV–Vis, FT-IR, ^{1}H NMR, and ^{13}C NMR, with NMR showing both *E* and *Z* isomers, indicating the configurational diversity of the products. Biological screening showed that all derivatives had moderate to strong antimicrobial properties, with the Mannich bases 6a and 6b being the most active. Antioxidant potency measured by the DPPH assay revealed that 5a and 6a displayed

relatively higher radical scavenging ability within the series. Brine shrimp lethality tests demonstrated dose-dependent cytotoxicity, suggesting general toxic potential of the synthesized compounds. Computational studies, including DFT-based geometry optimization, frontier molecular orbital analysis, molecular electrostatic potential mapping, and ADMET predictions, supported the experimental findings. These analyses indicated favorable electronic properties, good drug-likeness, and promising pharmacokinetic potential. Overall, these Schiff and Mannich base derivatives of 1,2,4-triazole, built on a natural phenolic acid scaffold, show potential as antimicrobial, antioxidant, and cytotoxic agents for further development.

AUTHORS CONTRIBUTION

Conceptualization: BS; Methodology: KB; Validation: BS; Investigation: KB; Data analysis: KB, BS; Writing-original draft: KB; Writing-review & editing: BS; Supervision: BS; Funding acquisition: none

FUNDING

None

ORCIDs

Bhushan Shakya:
https://orcid.org/0000-0003-1111-1382
Kishor Bhandari:
https://orcid.org/0009-0006-1210-8133

CONFLICT OF INTEREST

The authors declare that there are no conflicts of interest regarding the publication of this article.

DATA AVAILABILITY STATEMENT

The data that support the findings of this study are available from the corresponding author, upon reasonable request.

SUPPLEMENTARY INFORMATION

Figure S1. Synthesis and analytical data of target compounds
Figure S2–S9. ^{1}H and ^{13}C NMR spectra of target compounds

REFERENCES

Aggarwal, R., & Sumran, G. (2020). An insight on medicinal attributes of 1,2,4-triazoles. *European Journal of Medicinal Chemistry*, *205*, 112652. https://doi.org/10.1016/j.ejmech.2020.112652

Apu, A., Muhit, M., Tareq, S., Pathan, A., Jamaluddin, A., & Ahmed, M. (2010). Antimicrobial activity and brine shrimp lethality bioassay of the leaves extract of *Dillenia indica linn*. *Journal of Young Pharmacists : JYP*, *2*(1), 50–53. https://doi.org/10.4103/0975-1483.62213

Aryal, P., & Shakya, B. (2023). Synthesis, cytotoxicity, antibacterial and antioxidant activity of new 2-substituted benzimidazole containing 1,2,4-triazoles. *Journal of Nepal Chemical Society*, *43*(2), 34–45. https://doi.org/10.3126/jncs.v43i2.53339

Azim, T., Wasim, M., Akhtar, M. S., & Akram, I. (2021). An *in vivo* evaluation of anti-inflammatory, analgesic and anti-pyretic activities of newly synthesized 1, 2, 4 Triazole derivatives. *BMC Complementary Medicine and Therapies*, *21*(1), 304. https://doi.org/10.1186/s12906-021-03485-x

Bouamrane, S., Khaldan, A., Alaqarbeh, M., Sbai, A., Ajana, M. A., Lakhlifi, T., Bouachrine, M., & Maghat, H. (2024). Computational integration for antifungal 1,2,4-triazole inhibitors design: QSAR, molecular docking, molecular dynamics simulations, ADME/Tox, and retrosynthesis studies. *Chemical Physics Impact*, *8*, 100502. https://doi.org/10.1016/j.chphi.2024.100502

Brand-Williams, W., Cuvelier, M. E., & Berset, C. (1995). Use of a free radical method to evaluate antioxidant activity. *LWT - Food Science and Technology*, *28*(1), 25–30. https://doi.org/10.1016/S0023-6438(95)80008-5

Frieri, M., Kumar, K., & Boutin, A. (2017). Antibiotic resistance. *Journal of Infection and Public Health*, *10*(4), 369–378. https://doi.org/10.1016/j.jiph.2016.08.007

Kaur, R., Dwivedi, A. R., Kumar, B., & Kumar, V. (2016). Recent developments on 1,2,4-triazole nucleus in anticancer compounds: A review. *Anti-Cancer Agents in Medicinal Chemistry*, *16*(4), 465–489. https://doi.org/10.2174/1871520615666150819121106

Kurmi, S. P. C., & Karati, D. (2025). Insightful chemistry of molecular docking studies and ADMET profiling of 4-amino-1,2,4-triazole scaffolds as potential inhibitor of DprE1 enzymes as antitubercular agents. *Discover Chemistry*, *2*(1), 137. https://doi.org/10.1007/s44371-025-00208-w

Liu, M., Gopakumar, A., Hegde, V. I., He, J., & Wolverton, C. (2024). High-throughput hybrid-functional DFT calculations of bandgaps and formation energies and multifidelity learning with uncertainty quantification. *Physical Review Materials*, *8*(4), 043803. https://doi.org/10.1103/PhysRevMaterials.8.043803

Nediani, C., Ruzzolini, J., & Dinu, M. (2024). Oxidative stress and inflammation as targets for novel preventive and therapeutic approaches in non-communicable diseases III. *Antioxidants*, *13*(11), 1404. https://doi.org/10.3390/antiox13111404

Neupane, M. K., Sijapati Magar, B., Gurung, B., Lamichhane, R. R., & Pandey, P. (2025). Study

on the molecular dynamics of 2-(4-Fluorophenyl)-6-methyl-4-(3-(trifluoromethyl)phenyl)-1,2-dihydrodipyrazolo[3,4-b:3′,4′- *d*]pyridin-3(6 *H*)-one for cancer immunotherapy using a DFT Model. *ACS Omega*, acsomega.5c08756. https://doi.org/10.1021/acsomega.5c08756

Niksic, H., Becic, F., Koric, E., Gusic, I., Omeragic, E., Muratovic, S., Miladinovic, B., & Duric, K. (2021). Cytotoxicity screening of *Thymus vulgaris L.* essential oil in brine shrimp nauplii and cancer cell lines. *Scientific Reports*, *11*, 13178. https://doi.org/10.1038/s41598-021-92679-x

Osmaniye, D., Sağlık, B. N., Levent, S., Ilgın, S., Özkay, Y., & Kaplancıklı, Z. A. (2021). Design, synthesis, in vitro and in silico studies of some novel triazoles as anticancer agents for breast cancer. *Journal of Molecular Structure*, *1246*, 131198. https://doi.org/10.1016/j.molstruc.2021.131198

Parr, R. G., & Yang, W. (2020). *Density-functional theory of atoms and molecules*. Oxford University Press. https://doi.org/10.1093/oso/9780195092769.001.0001

Peng, Z., Wang, G., Zeng, Q.-H., Li, Y., Wu, Y., Liu, H., Wang, J. J., & Zhao, Y. (2021). Synthesis, antioxidant and anti-tyrosinase activity of 1,2,4-triazole hydrazones as antibrowning agents. *Food Chemistry*, *341*, 128265. https://doi.org/10.1016/j.foodchem.2020.128265

Pires, D. E. V., Blundell, T. L., & Ascher, D. B. (2015). pkCSM: predicting small-molecule pharmacokinetic and toxicity properties using graph-based signatures. *Journal of Medicinal Chemistry*, *58*(9), 4066–4072. https://doi.org/10.1021/acs.jmedchem.5b00104

Pooja, G., Shweta, S., & Patel, P. (2025). Oxidative stress and free radicals in disease pathogenesis: A review. *Discover Medicine*, *2*(1), 104. https://doi.org/10.1007/s44337-025-00303-y

Qi, L., Wu, S., Li, M., Bai, J., Ma, H., & Ren, Y. (2020). Synthesis, biological activity, and molecular docking studies of novel 5-Substituted-1,2,4-Triazole-3-thione derivatives. *ChemistrySelect*, *5*(6), 2015–2022. https://doi.org/10.1002/slct.201904418

Rouzi, K., Brandán, S. A., El Houssni, I., Poyraz, E. B., Hassani, I. A. E., Dege, N., Abuelizz, H. A., Oulmidi, A., Bouatia, M., & Karrouchi, K. (2025). 4-amino-5-(pyridin-4-yl)-4*H*-1,2,4-triazole-3-thiol as potent antimicrobial agent: Synthesis, X-ray, antimicrobial activity and computational studies. *Journal of Molecular Structure*, *1320*, 139613. https://doi.org/10.1016/j.molstruc.2024.139613

Sadeghian, S., Emami, L., Mojaddami, A., khabnadideh, S., Faghih, Z., Zomorodian, K., Rashidi, M., & Rezaei, Z. (2023). 1,2,4-Triazole derivatives as novel and potent antifungal agents: Design, synthesis and biological evaluation. *Journal of Molecular Structure*, *1271*, 134039. https://doi.org/10.1016/j.molstruc.2022.134039

Tyagi, P., Tyagi, M., Agrawal, S., Chandra, S., Ojha, H., & Pathak, M. (2017). Synthesis, characterization of 1,2,4-triazole Schiff base derived 3d- metal complexes: Induces cytotoxicity in HepG2, MCF-7 cell line, BSA binding fluorescence and DFT study. *Spectrochimica Acta Part A: Molecular and Biomolecular Spectroscopy*, *171*, 246–257. https://doi.org/10.1016/j.saa.2016.08.008

Wang, A., Kingsbury, R., McDermott, M., Horton, M., Jain, A., Ong, S. P., Dwaraknath, S., & Persson, K. A. (2021). A framework for quantifying uncertainty in DFT energy corrections. *Scientific Reports*, *11*(1), 15496. https://doi.org/10.1038/s41598-021-94550-5

WHO bacterial priority pathogens list, 2024: Bacterial pathogens of public health importance to guide research, development and strategies to prevent and control antimicrobial resistance. (n.d.). Retrieved August 12, 2025, from https://www.who.int/publications/i/item/9789240093461

Wu, S., Qi, L., Ren, Y., & Ma, H. (2020). 1,2,4-triazole-3-thione Schiff bases compounds: Crystal structure, hirshfeld surface analysis, DFT studies and biological evaluation. *Journal of Molecular Structure*, *1219*, 128591. https://doi.org/10.1016/j.molstruc.2020.128591

Wu, S., Zhang, W., Qi, L., Ren, Y., & Ma, H. (2019). Investigation on 4-amino-5-substituent-1,2,4-triazole-3-thione Schiff bases an antifungal drug by characterization (spectroscopic, XRD), biological activities, molecular docking studies and electrostatic potential (ESP). *Journal of Molecular Structure*, *1197*, 171–182. https://doi.org/10.1016/j.molstruc.2019.07.013

Yang, P., Luo, J.-B., Wang, Z.-Z., Zhang, L.-L., Feng, J., Xie, X.-B., Shi, Q.-S., & Zhang, X.-G. (2021). Synthesis, molecular docking, and evaluation of antibacterial activity of 1,2,4-triazole-norfloxacin hybrids. *Bioorganic Chemistry*, *115*, 105270. https://doi.org/10.1016/j.bioorg.2021.105270

Zhu, P., Zhou, T., Chen, H., Chen, X., Wang, X., Kong, L., & Yang, M. (2023). Novel triazoles with potent and broad-spectrum antifungal activity *in vitro* and *in vivo*. *Journal of Medicinal Chemistry*, *66*(11), 7497–7515. https://doi.org/10.1021/acs.jmedchem.3c00266